Control of Second Life Hybrid Battery Energy Storage System based on Modular Boost-Multilevel Buck Converter

Abstract- **To fully utilize second life batteries on the grid system a hybrid battery scheme needs to be considered for several reasons; the uncertainty over using a single source supply chain for second life batteries, the differences in evolving battery chemistry and battery configuration by different suppliers to strive for greater power levels and the uncertainty of degradation within a second life battery. Therefore, these hybrid battery systems could have widely different module voltage, capacity, initial SOC and state-of-health (SOH). In order to suitably integrate and control these widely different batteries, a suitable multi-modular converter topology and associated control structure are required. This paper addresses these issues proposing a modular boost-multilevel buck converter based topology to integrate these hybrid second life batteries to a grid-tie inverter. Thereafter, a suitable module based distributed control architecture is introduced to independently utilise each converter module according to its characteristics. The proposed converter and control architecture are found to be flexible enough to integrate widely different batteries to an inverter dc-link. Modelling, analysis and experimental validation are performed on a single phase modular hybrid battery energy storage system prototype to understand the operation of the control strategy with different hybrid battery configurations.**

Index Terms—**Second life hybrid batteries, modular boost-multilevel buck converter, distributed control strategy, boost-buck control mode.**

NOMENCLATURE

$V_{batt,i}$	: Battery terminal voltage of ith module	(V)
$i_{batt,i}$	: Battery current of ith module	(A)
ω_i	: Desired weighting factor for i^{th} module current	
$i_{dc,i}$	: Instantaneous dc-link current of ith module	(A)
$I_{dc,i}$	: Steady state dc-link current of ith module	(A)
$V_{dc,i}$	: Dc-link capacitor voltage of ith module	(V)
$V_{dc,m}^{*}$	: Desired module dc-link capacitor voltage	(V)
$\widehat{i_{batt,i}}$	: Small signal value of ith module current	(A)
$\widehat{V_{dc,i}}$	: Small signal i^{th} module dc-link voltage	(V)
V_{dc}^{*}	: Desired central DC-link capacitor voltage	(V)
I_{dc}	: Average DC-link current	(A)
i_{dc}	: Instantaneous value of DC-link current	(A)
V_{sw}	: Maximum switch voltage rating of module	(V)
d_i	: Instantaneous duty cycle of switches S_i, S_{ii}	
d_{av}	: Overall duty cycle of multilevel buck converter	
$d_{i\,i}$	: Instantaneous duty cycle of switches T_i, T_{ii}	
D_i	: Average duty cycle of switches S_i, S_{ii}	
D_{ii}	: Average duty cycle of switches T_i, T_{ii}	
C	: Module dc-link capacitance	(F)
L	: Module boost inductance	(H)
L_{dc}	: Dc-link inductor	(H)
R	: leakage resistance of the boost inductor/module	(Ω)
R_{dc}	: leakage resistance of the dc-link inductor	(Ω)
$Q_{max,i}$	: Battery capacity of the ith module	(Ah or C)
$OCV_{0,i}$	: Initial open circuit voltage of ith battery module	(V)

I. INTRODUCTION

Significant research has been carried out on battery energy storage systems (BESS) using a single type of battery with homogeneous characteristics where a single dc-dc or dc-ac converter interface with the battery bank is used both in grid-tie and in microgrid applications [1] − [4]. This paper is concerned with hybrid second life battery systems e.g. re-using EV/HEV batteries in grid support applications because there is a significant interest in using these transportation batteries to help support the new smart grid functionalities [5] − [7]. The main advantage of these batteries are the supposed lower cost and the chance to delay the development of the second life battery recycling chain which is in its infancy due to changing battery chemistry and the impact on the recycling process cost. These second life batteries are likely to trickle through the battery recyclers (at a module level) and therefore to get a sufficiently large system for grid support will require the use of different manufacturer's batteries. Each battery in the system could have a different chemistry, voltage, capacity, initial State of Charge (SOC). As a battery fails it would be desirable to *hot-swap* it for one that works resulting in a hybrid mix encompassing everything from new batteries to batteries close to failure at any moment in time.

To meet the requirements for integrating together hybrid energy storage systems, multi-modular power converters (cascaded/parallel) are preferred [8] − [9]. Previous research on such hybrid energy systems with batteries has mainly focused on generation-storage hybridization for example; batteries with super-capacitor, batteries with PV/wind or fuel cells [10] − [12]. These researches use the same type of battery system and focus on power sharing between the battery and other sources to increase battery useful life or smoothing the mismatch between the generation and demand.

In some cases, multi-modular converters are also used for power sources of the same type but under different operating conditions. For example, they can be used for PV systems under partial shading [13] − [14] using multi-modular dc-dc converters with a single inverter to deal with the heterogeneous nature of PV panels under MPPT conditions. Several authors have compared and recommended cascaded dc-dc converters over a parallel structure due to increased efficiency and reduced size and/or cost [13]. In that research, boost type modules were preferred for low module voltages where the total dc-side voltage is less than the inverter dc-link voltage, whereas buck type modules were suggested for the case of higher module voltages (higher than the inverter dc-link). From a control point of view, a cascaded boost converter

neither can deliver the peak power from a module under all inhomogeneous radiation conditions, nor can it provide the fault tolerance without extra protection, whereas a cascaded buck structure is capable of handling both situations. In order to address the shortfall of a cascaded boost structure, a separate string diverter was proposed in [15] which could solve power mismatch problems but not the problem of integrating widely uneven module voltages together. Therefore, these three problems: a) integrating widely different voltage modules to an inverter dc-link b) fault-tolerance and *hot-swapping* and c) distributed utilisation of different modules have been looked at in different contexts but not together in a hybrid energy system.

These are important and relevant issues in second life battery integration as the vehicle batteries, for example, come in the range of 12/24V up to 600V with ratings of 0.5kWh up to 50kWh. The smallest accessible module may be anything from a cell to a complete system. As a result, depending on the battery availability, the overall battery side voltage can be greater or less than the desired dc-link voltage of the line side inverter under normal operation which makes it difficult to integrate them to a common inverter dc-link using either a boost or a buck type modular converter. Moreover, in order to control these hybrid batteries according to their characteristics each module may need to be charged or discharged at significantly different current levels within the converter. As a result, the integration of such hybrid batteries is challenging both in terms of converter topology and control.

There are no research reports to date about the power converter interface and control issues to integrate widely different battery types (new/second life) into a single grid-tie converter. To overcome these shortfalls, this paper proposes a modular boost-multilevel buck dc-dc converter topology based on a cascaded structure to integrate hybrid second life battery modules to a common inverter dc-link irrespective of their voltage levels and characteristics. Moreover, a generalised distributed control structure has been introduced for the proposed converter which allows control of each converter module independently through a weighting function to optimally utilize different battery modules depending on their relative characteristics within a set of hybrid batteries. The paper is structured as follows: converter topology is presented in section II, dynamic modeling, power sharing and distributed control structure are given in section III, section IV and section V respectively. The experimental validation is provided in section VI and section VII concludes the paper.

II. CONVERTER TOPOLOGY

This paper describes an H-bridge cascaded boost-multilevel dc-dc converter based topology with an inverter as shown in Fig. 1. This topology offers a good compromise between the cost, efficiency and reliability while maintaining the flexibility to deal with different battery voltages and power levels. By choosing an H-Bridge module, the converter can be operated in any of boost, buck and boost-buck mode by independently controlling the two legs of an H-bridge to enable different battery voltages to be dealt with for a required dc bus voltage

with a narrow voltage range for grid inversion.

A boost type module is generally considered when all the dc-sources, be they, generation or batteries have low voltages which meets the condition $\sum V_{batt,i} < V_{dc}^*$. However, this structure is not fault-tolerant and has an inherent current limitation ($i_{batt,i} \geq I_{dc}$) which makes them unsuitable when module currents demand to be lower the dc-link current.

On the other hand, a Buck type module could be used only when all the dc-sources meet the condition $\sum V_{batt,i} > V_{dc}^*$. The main advantages of a buck type module are: a) the ability to utilise a module better than a boost module because it is possible to make $i_{batt,i} \leq I_{dc}$, b) fault-tolerant in nature (does have module bypassing capability). However, there are some limitations of this mode also which includes the need for a large number of modules if only low voltage batteries are available and the input current is discontinuous which adds the requirement for a high input capacitor across each battery module which increases the overall system size and cost.

A buck-boost module configuration has previously been compared to a boost and buck configuration for systems with mixed voltages [13]. The author concluded that there was poor switch utilization, low converter efficiency, large capacitors on both inputs and outputs which possibly increase the module size/cost and reduces the reliability of a converter module. Moreover, the requirement of different switch rating/module makes the module selection and design difficult.

In order to overcome the above drawbacks, a modular boost-multilevel buck configuration is used with a single multi-switch buck converter. The proposed configuration uses a boost module with each battery bank and then adds a half-bridge in parallel with each module capacitor to make it fault-tolerant in boost mode and provide an opportunity to switch in the buck mode (if needed). Thereafter, these half-bridges are connected in cascade through a single inductor to integrate all the modules to a common dc-link voltage as shown in Fig 1(a). Due to having a boost module at the input of each module, it can avoid an input capacitor due to the continuous current and the overall design of a module becomes easier because of the uniform voltage rating for all the devices.

A. Principle of Operation

Each input converter (S_i, S_{ii}) can work in PWM mode to form the module capacitor voltages $V_{dc,1}$, $V_{dc,2}$ …$V_{dc,n}$ and then the cascaded half-bridge switches (T_i, T_{ii}) can be operated as a multilevel buck converter [16] to maintain the desired central dc-link voltage (V_{dc}). In this way, the converter behaves as a two-stage dc-dc converter as indicated in Fig 1(a). The topology configuration offers a large degree of flexibility, using an appropriate combination of module switches (S_i, S_{ii} and T_i, T_{ii}) where each module may be operated in boost (buck module bypassed, T_i, T_{ii} in idle), in buck mode (with the boost module bypassed, S_i, S_{ii} in idle) or in boost-buck mode (S_i, S_{ii} and T_i, T_{ii} in PWM) as shown in Table I. The application range, expressed as $\sum V_{batt,i}$ against the control flexibility (as a range of $i_{batt,i}$) has been shown in Fig 1(b) to understand the operational envelope of the proposed converter in different modes. It can be seen from Fig 1(b) that the boost and the buck mode offer a narrow operating envelope on the plane.
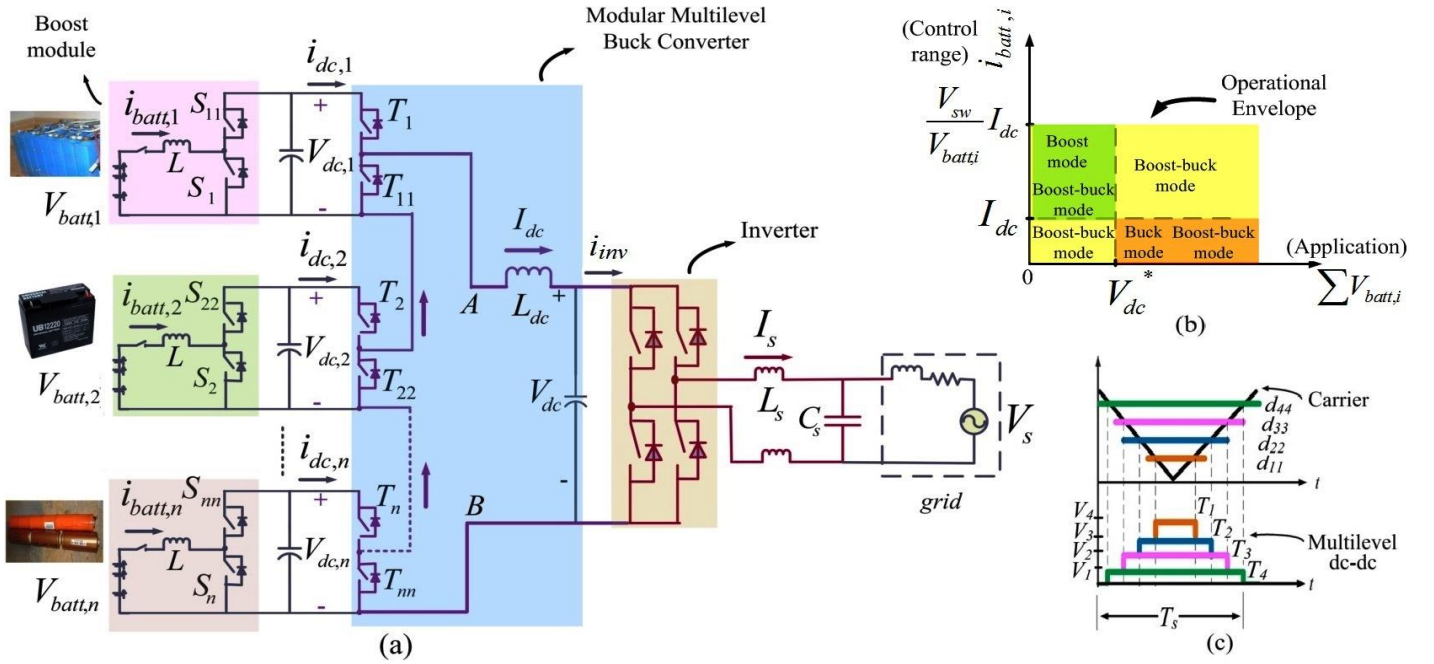
Fig. 1 Proposed converter for single phase second life hybrid battery energy storage system: a) power circuit, b) operational envelope, c) multilevel operation

TABLE I
DIFFERENT POSSIBLE MODES OF THE PROPOSED CONVERTER

Possible Modes	Switching of S_i, S_{ii}	Switching T_i, T_{ii}	Overall operation and range of control
1	S_i and S_{ii} in PWM mode ($\forall i = 1..n$)	T_i and T_{ii} in idle mode (T_i is ON, T_{ii} is OFF) ($\forall i = 1..n$)	Cascaded Boost Range - ($i_{batt,i} \geq I_{dc}$)
2	S_i and S_{ii} in idle mode (S_i is OFF, S_{ii} is ON) ($\forall i = 1..n$)	T_i and T_{ii} in PWM mode ($\forall i = 1..n$)	Multilevel buck Range -($i_{batt,i} \leq I_{dc}$)
3	S_i and S_{ii} in PWM ($\forall i = 1..n$)	T_i and T_{ii} in PWM mode ($\forall i = 1..n$)	Boost- multilevel buck Range - ($i_{batt,i} \leq I_{dc}$) ($i_{batt,i} \geq I_{dc}$)
4	S_i and S_{ii} in idle	T_i and T_{ii} in bypass mode (T_i is OFF and T_{ii} is ON)	Bypass i^{th} module

The boost mode suffers from a current limitation problem while a buck mode has an inherent voltage limitation issue. The boost-buck mode provides a wide control flexibility ($i_{batt,i} \geq I_{dc}$ and $i_{batt,i} \leq I_{dc}$) over any application range ($\sum V_{batt,i} > V_{dc}^*$ and $\sum V_{batt,i} \leq V_{dc}^*$) within a pre-defined design envelope. Therefore, this mode is more suitable to integrate widely different characteristics batteries to an inverter dc-link. Within each module the battery cells have balancing circuits similar to [17] – [18] in order to uniformly utilise each cell in a module.

B. Module Design

The design of an H-bridge module, inductor and capacitor is challenging because of the uneven module voltages and potential variation of module current. There are two approaches: a) designing different module switch ratings and inductor/capacitor values according to individual module battery parameters or b) designing a uniform switch rating and inductor/capacitor by pre-defining a maximum battery voltage and current envelope. The latter approach has been followed in this work because different switch rating and passive

component ratings in different modules complicates the design of the modular converter and prevents hot-swapping of a battery module. A battery size envelope was used to choose the appropriate switch rating. The boost inductor was chosen to give a maximum of 5% current ripple as calculated in (1) where D_{max} is the maximum duty cycle, $\Delta i_{batt,i}$ is the magnitude of the ripple current, T_s is the switching time and V_{sw} is the maximum switch voltage rating. V_{sw} is chosen to be 5 the times maximum battery voltage (to account for a reasonable boost ratio and a margin of around 20%).

$$L = \left(1 - \frac{\max(V_{batt,i})}{V_{sw}}\right) \times \frac{\max(V_{batt,i})}{0.05 \times \max(i_{batt,i})} T_s \qquad (1)$$

Similarly, the design of the module capacitor was set to correspond to a maximum allowable voltage ripple, ΔV, on the module (set to 1% of the dc-bus voltage) as shown in (2).

$$C = \left(1 - \frac{\max(V_{batt,i})}{V_{sw}}\right) \frac{I_{dc}}{\Delta V} T_s, \ \Delta V = 0.01 \times \max(V_{dc,i}) \qquad (2)$$

III. CONVERTER MODELLING

The dynamic modelling of the converter in Fig 1(a) is composed of two-stages: a) modelling input boost converter, b) modelling of modular multilevel buck converter.

A. Input side boost converter

The dynamic equations for the input side boost converter can be written as follows considering *n* converter modules:

$$L \frac{di_{batt,i}}{dt} + Ri_{batt,i} + (1 - d_i)V_{dc,i} = V_{batt,i} \ \forall i = 1 \dots n \qquad (3)$$

$$C \frac{dV_{dc,i}}{dt} - (1 - d_i)i_{batt,i} = -i_{dc,i} \ \forall i = 1 \dots n \qquad (4)$$

$$\langle V_{dc,i} \rangle_{av} = \frac{1}{1 - D_i} V_{batt,i} \ \forall i = 1 \dots n \qquad (5)$$

It is necessary to investigate the model to accurately predict the dynamics of the control system. The required small model can be expressed by the state-space equations as shown in (6) employing two state-variables $V_{dc,i}$ and $i_{batt,i}$ per module.

$$\dot{X} = \begin{pmatrix} -\frac{R}{L} & -\frac{(1-D_i)}{L} \\ \frac{(1-D_i)}{C} & 0 \end{pmatrix} X + \begin{pmatrix} \frac{1}{L} & \frac{V_{dc,i}}{L} & 0 \\ 0 & -\frac{i_{batt,i}}{C} & -\frac{1}{C} \end{pmatrix} U \ \forall i = 1 \ldots n$$

Where, $X = \begin{pmatrix} \widehat{i_{batt,i}} \\ \widehat{V_{dc,i}} \end{pmatrix}, U = \begin{pmatrix} \widehat{V_{batt,i}} \\ \widehat{d_i} \\ \widehat{I_{dc,i}} \end{pmatrix}$ (6)

B. Multilevel Buck Converter

The cascaded switches $T_i, T_{ii} \ \forall i = 1 \ldots n$ at the output of each boost converter work as a combined buck converter along with the dc-link inductor as highlighted in Fig 1(a). Each of these switches can have an individual duty ratio d_{ii} and an overall average duty ratio d_{av} of the buck converter. This d_{ii} controls each module current $i_{batt,i}$ through $i_{dc,i}$ while d_{av} maintains the central dc-link voltage (V_{dc}) irrespective of d_{ii}. The dynamic equations can be written as follows:

$$L_{dc}\frac{d i_{dc}}{dt} + R_{dc}i_{dc} + V_{dc} = d_{av}\sum V_{dc,i} \ \forall i = 1 \ldots n \tag{7}$$

$$d_{av} = \frac{V_{dc}}{\sum V_{dc,i}} = \frac{\langle \sum V_{dc,i} d_{ii} \rangle}{\sum V_{dc,i}} \ \forall i = 1 \ldots n \tag{8}$$

$$I_{dc,i} = D_{ii}I_{dc} \ \forall i = 1 \ldots n \tag{9}$$

$$C_{dc}\frac{dV_{dc}}{dt} = i_{dc} - i_{inv} \tag{10}$$

The state-space model of multilevel buck converter can be written as following:

$$(\dot{X}) = \begin{pmatrix} -\frac{R_{dc}}{L_{dc}} & -\frac{1}{L_{dc}} \\ \frac{1}{C_{dc}} & 0 \end{pmatrix}(X) + \begin{pmatrix} \frac{D_{av}}{L} & \frac{\sum V_{dc,i}}{L} & 0 \\ 0 & 0 & -\frac{1}{C_{dc}} \end{pmatrix}(U) \ \forall i = 1 \ldots n$$

Where $X = \begin{pmatrix} \widehat{i_{dc}} \\ \widehat{V_{dc}} \end{pmatrix}, U = \begin{pmatrix} \widehat{\sum V_{dc,i}} \\ \widehat{d_{av}} \\ \widehat{i_{inv}} \end{pmatrix}$ (11)

C. Control Range of the Converter

The control range of the converter is essentially the relationship between $i_{batt,i}$ and I_{dc} because it provides an information about the converter operating range as shown in Fig 1(b). The power balance equation can be used to find this relationship using (12) where η_i is the efficiency of the associated boost converter.

$$V_{dc,i}i_{dc,i} = \eta_i V_{batt,i}i_{batt,i} \ \forall i = 1 \ldots n \tag{12}$$

$$D_{ii}I_{dc} = \frac{V_{batt,i}}{V_{dc,i}}I_{batt,i} = (1 - D_i) I_{batt,i} \ \forall i = 1 \ldots n \tag{13}$$

$$I_{batt,i} = \frac{D_{ii}}{(1-D_i)} I_{dc} \ \forall i = 1 \ldots n \tag{14}$$

It can be seen from (14) that a module current can be controlled to more or less than the dc-link current (I_{dc}) using an appropriate combination of D_i and D_{ii}. If $I_{batt,i} > I_{dc}$ then the condition $(D_{ii} + D_i) > 1$ needs to be satisfied. For $I_{batt,i} < I_{dc}$ the condition $(D_{ii} + D_i) < 1$ needs to be fulfilled.

IV. POWER SHARING STRATEGY

The control/power sharing of modular energy storage systems has been done previously using a single type of batteries or super-capacitor concentrating on the balancing control e.g. voltage/SOC among the modules [19] – [20]. A distributed power sharing was performed in mainly PV system where the modular dc-dc converters were controlled according to the distributed MPPT [21] – [22]. However, the major differences between PV systems and a hybrid battery system are: a) control architecture in PV system is mainly unidirectional whereas in BESS it has to be bidirectional, b) the criteria for distributing the power between modules is dependent on multiple battery parameters such as, voltage, capacity etc. unlike in PV system which is solely dependent on different radiation conditions.

The distributed sharing proposed in the paper is based on weighting factors (ω_i) which represent the status ("goodness" or "badness") of each battery module on an instantaneous basis as presented in (15). Since each of these hybrid module types will charge/discharge at different rates and have different maximum/minimum safe amounts of charge and voltages, the weighting factor based strategy ensures that the charging/discharging trajectory of the hybrid modules during a charging or discharging cycle will all arrive at their maximum or minimum values at the same time. The detailed derivation of the weighting factor is presented in the Appendix.

$$\frac{i_{batt,1}}{\omega_1} = \frac{i_{batt,2}}{\omega_2} = \cdots = \frac{i_{batt,n}}{\omega_n}, \omega_i = f\left(V_{batt,i}, OCV_{0,i}, Q_{max,i}\right) \tag{15}$$

V. DISTRIBUTED CONTROL ARCHITECTURE

Since the relative weighting factors (i.e. ω_i: ω_j) can be significantly different in this hybrid battery integration, the proposed control structure employs the boost-buck control mode to achieve a wide operational envelope as shown in Fig 1(b). The main objectives of the control architecture are: a) to control the central dc-bus V_{dc} to a fixed value irrespective of set of batteries present to allow the line side inverter to respond according to the desired grid side power demand, b) to control the hybrid battery modules according to the desired battery weighting factors to optimally utilise them.

The principle concept of the proposed distributed control is to control the input side boost converters (S_i, S_{ii}) to form equal module dc-link voltages irrespective of their input voltages and then utilise a concept of distributed duty ratio ($d_{ii} \forall i = 1 \ldots n$) of the buck converter switches (T_i, T_{ii}) as a function of battery weighting factors (ω_i). This control operation makes the converter behave as a multilevel converter as indicated by the effect of the different module duty ratio's in Fig 1(c). There could be two possible cases depending on the set of batteries present: a) a similar set of batteries present, b) a widely different batteries present. Two different control techniques have been described.
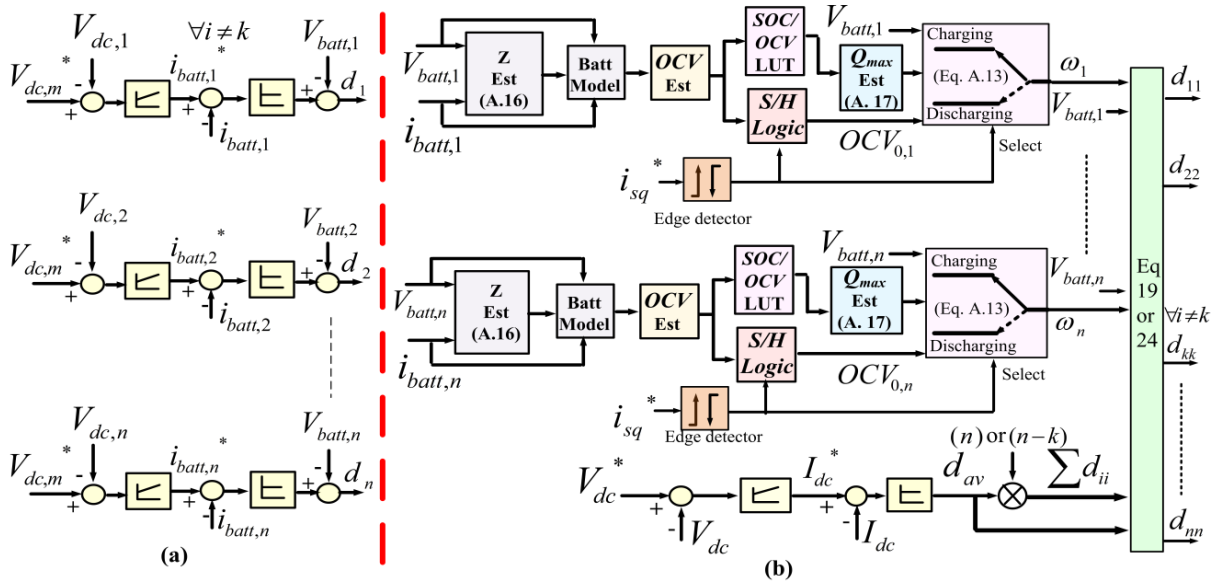
Fig 2 Proposed dc-side distributed control architecture of the converter: a) module boost converter control, b) multilevel buck converter control

A. Case 1 – All modules in boost-buck mode (dc-side control)

This control is used where all the modules are operated in boost-buck mode, e.g. all modules have similar voltages 12V with 24V etc. The module input voltages are boosted to $V_{dc,1}$, $V_{dc,2}$ … $V_{dc,n}$ using the input side boost converters (S_i, S_{ii} $\forall i = 1 \dots n$) and then the overall voltage ($\sum V_{dc,i}$) is bucked using the multilevel buck converter (T_i, T_{ii}) to maintain the central inverter dc-link voltage constant at the time. All the module boost converters are controlled to a same voltage reference $V_{dc,m}{}^*$ independent of the weighting factors where the upper limit is limited by the maximum switch rating V_{sw} of a module as shown in (16). The desired module independent control is achieved using the duty ratios $d_{ii} \forall i = 1 \dots n$. The derivation is presented in (17) – (19) using (12) assuming $\eta_i \approx 1$.

$$nV_{dc,m}{}^* > V_{dc}{}^* \rightarrow \frac{V_{dc}{}^*}{n} < V_{dc,m}{}^* \leq V_{sw} \qquad (16)$$

From (12), $V_{dc,i}i_{dc,i} = V_{dc,m}(d_{ii})I_{dc} \approx V_{batt,i}i_{batt,i}$ therefore,

$$d_{ii} \propto V_{batt,i}i_{batt,i} \, \forall i = 1 \dots n \text{ for a constant } I_{dc} \qquad (17)$$

From (15), if $i_{batt,i} \propto \omega_i \, \forall i = 1 \dots n$ then from (17)

$$d_{ii} \propto \omega_i V_{batt,i} \forall \, i = 1 \dots n \qquad (18)$$

According to (8), $d_{av} = \frac{\sum V_{dc,i}d_{ii}}{\sum V_{dc,i}}$

After putting $V_{dc,i} = V_{dc,m} \quad \forall i = 1 \dots n$ in (8)

$$d_{av} = \frac{V_{dc,m}(\sum d_{ii})}{nV_{dc,m}} \rightarrow \sum d_{ii} = nd_{av}$$

Therefore, $d_{ii} = nd_{av}\frac{\omega_i V_{batt,i}}{\sum_{i=1}^{n} \omega_i V_{batt,i}} \, \forall i = 1 \dots n \qquad (19)$

B. Case 2 –Boost-k out of n modules only in buck mode (dc-side control)

This dc-side control is different, where not all the modules can operate in boost-buck mode. For example, where the battery module voltages are considered to be substantially different e.g. 24V with 220V etc. or when the switch rating is not sufficiently high enough to allow the boost operation of a higher voltage connected battery. A control strategy to deal with this is: a) to operate the higher input voltage module only in buck mode with the corresponding boost converters (k) in idle mode which means S_k, S_{kk} in idle ($V_{dc,k} = V_{batt,k}$) and T_k, T_{kk} in PWM, b) to operate the remaining modules ($n–k$) in boost-buck mode as previously described which means S_i, S_{ii} in PWM and T_i, T_{ii} in PWM $\forall i \neq k$. The module voltage reference ($V_{dc,m}{}^*$) is calculated in (20) and the duty ratio distribution is derived in (21) to (24).

$$\frac{(V_{dc}{}^* - \sum_{k \neq i} V_{batt,k})}{(n-k)} < V_{dc,m}{}^* < V_{sw} \, \forall i \neq k \qquad (20)$$

From (12), $V_{dc,i} = V_{dc,m}$, $d_{ii} \propto \omega_i V_{batt,i} \, \forall i \neq k = 1 \dots n$

For the (k) modules in buck mode, from (12);

$$V_{dc,k} = V_{batt,k}, \, V_{batt,k}i_{dc,k} = V_{batt,k}i_{batt,k} \rightarrow d_{kk} \propto \omega_k \quad (21)$$

Now with the help of (8), following expressions are derived:

$$V_{dc,m} \sum_{i \neq k} d_{ii} + \sum_k V_{batt,k}d_{kk} = d_{av}\left((n - k)V_{dc,m} + \sum_k V_{batt,k}\right) \qquad (22)$$

Equating, $V_{dc,m} \sum_{i \neq k} d_{ii} = d_{av}(n - k)V_{dc,m}$ and

$\sum_k V_{batt,k}d_{kk} = d_{av} \sum_k V_{batt,k}$ the following can be written,

$$\sum_{i \neq k} d_{ii} = (n - k)d_{av} \text{ and } d_{av} = \frac{\sum_k V_{batt,k}d_{kk}}{\sum_k V_{batt,k}} \qquad (23)$$

Now using (18) and (21) the following expressions can be derived

$$d_{ii\,(i\neq k)} = (n-k)d_{av}\frac{\omega_i V_{batt,i}}{\sum_{i\neq k}\omega_i V_{batt,i}} \text{ and}$$

$$d_{kk} = d_{av}\frac{\omega_k\sum_k V_{batt,k}}{\sum_k\omega_k V_{batt,k}} \text{ Where } d_{kk} = d_{av} \text{ for } k=1 \qquad (24)$$

C. Overall Control Structure

The detailed control structures for both the dc-side and the ac-side are shown in Fig 2 and Fig 3 respectively. The dc-side control (Fig 2) is composed of two-stages: a) control of the boost converter and b) control of the multilevel buck converter. The module boost converters are controlled by the same voltage reference ($V_{dc,m}{}^*$) using an outer PI-voltage loop and an P-inner current loop. The selection of this reference is done using (16) or (20). The proposed control structure of the multilevel buck converter is shown in Fig 2(b). It consists of two-stages: i) battery parameter estimation and weighting factor generation and ii) closed loop control. The control employs a central dc-bus voltage loop and the output of that controller provides the overall duty ratio (d_{av}) command through an inner dc-link current controller. Thereafter, this d_{av} is split into module duty ratios (d_{ii}) using (19) or (24) which maintains V_{dc} as well as control the module currents in the desired manner. The grid side control (Fig 3) depends on the type of application of the energy storage system e.g. voltage control or the frequency control. The output of the voltage or frequency controller provides the reference for the inner q-axis (active power axis) current loop. The d-axis is taken as the reactive power axis. This $i_{sq}{}^*$ plays an important role because the weighting factor for charging and discharging is different on the dc-side. The sign of $i_{sq}{}^*$ indicates the phase of line side current with respect the line voltage. Therefore, this dynamic change-over is performed using the sign of $i_{sq}{}^*$ though an edge detector as shown in Fig 2(b). The initial OCV is updated at the end of charging and discharging cycle. This is performed through a sample and hold (S/H) logic and an edge detector using the $i_{sq}{}^*$.
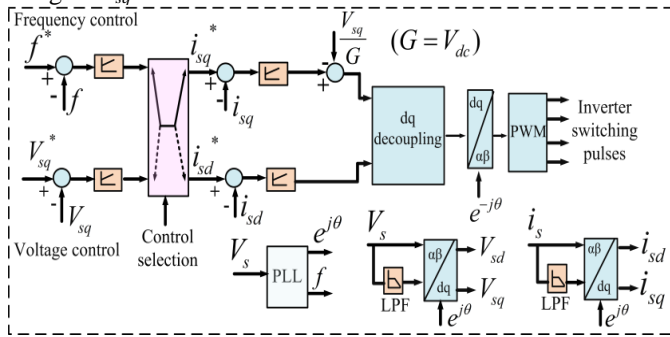

Fig 3 Line side inverter control structure for grid support application

VI. EXPERIMENTAL INVESTIGATION

A four-module or five-level hybrid battery energy storage system has been built as shown in Fig 4 and tested in a grid connected condition to validate the proposed control. Different converter modules contain different batteries in terms of chemistry/type, voltage, capacity. Initial characterizations such as pulse load tests [25] have been performed to find the parameters of a module before putting it into a converter

module as shown in Table II. The inverter was controlled to meet a fixed grid side power demand.
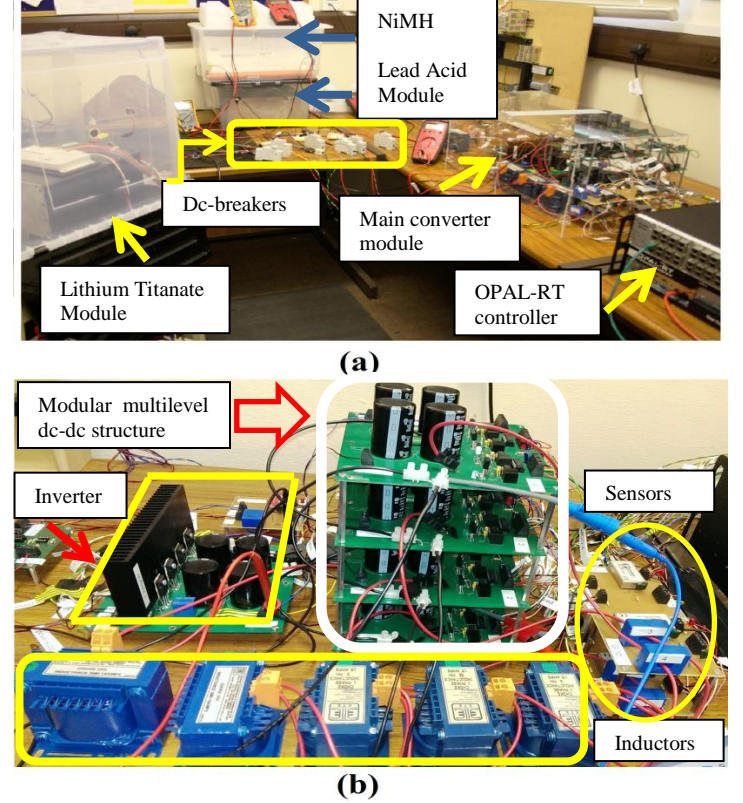

(a)

(b)

Fig 4 Multi-modular hybrid prototype: a) overall set-up, b) converter module

TABLE II
COMPONENTS AND THEIR SPECIFICATIONS IN EXPERIMENTAL VALIDATION

Type/Name	Rating/specification
OptiMOS for H-bridge dc-dc modules	100V 40A – (FDPF085N10A)
Boost inductors of dc-dc modules (L)	1.5mH, 15A, $R_L = 20m\Omega$
dc-link inductor (L_{dc})	3mH, 15A, $R_L = 40m\Omega$
module dc-link capacitors	2200µF, 100V
Switching frequency of the dc-dc module and inverter	10kHz
module dc-link voltage ($V_{dc,m}$)	80V
Operating central dc-bus voltage (V_{dc})	150V
Line side filters (L_s, C_s)	3mH, 3mH and 10 µF
Nominal Grid voltage (V_s)	120V (peak), 50Hz
Test power command (P)	450W
Battery module – 1 (lead acid)	12V, 10Ah– $V_{max} = 14V$ $V_{min} = 9.5V$, Initial Z = 0.015Ω
Battery module – 2 (lithium titanate)	24V, 60Ah– $V_{max} = 27V$ $V_{min} = 18V$, Initial Z = 0.006Ω
Battery module – 3 (NiMH)	7.2V, 6.5Ah, $V_{max} = 8.5V$, $V_{min} = 5V$, Initial Z = 0.01Ω
Battery module – 4 (lead acid)	24V (2x12V), 16Ah lead acid – $V_{max} = 18V$ $V_{min} = 28V$, Initial Z = 0.022Ω

A. Multilevel Operation

In order to show the multilevel operation of the converter, the voltage V_{AB} in Fig 1(a) is measured. Since all the switches T_i, T_{ii} operate in different duty ratio depending on weighting factors, this voltage varies between zero and a combination of the different voltage levels e.g. $V_{dc,m}$, $2V_{dc,m}$, $3V_{dc,m}$, $4V_{dc,m}$ at switching frequency. Fig 5a shows this operation. It can be seen that there is five distinct voltage levels of the converter.
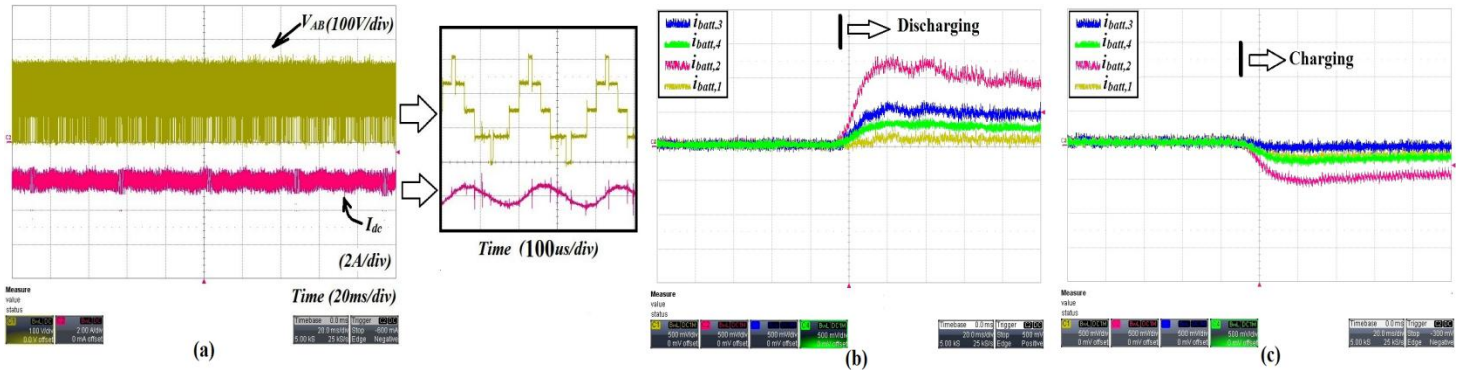
Fig 5 Experimental result of converter operation: a) multilevel operation, b) zero to discharging, c) zero to charging scale time 20ms/div, module currents 5A/div
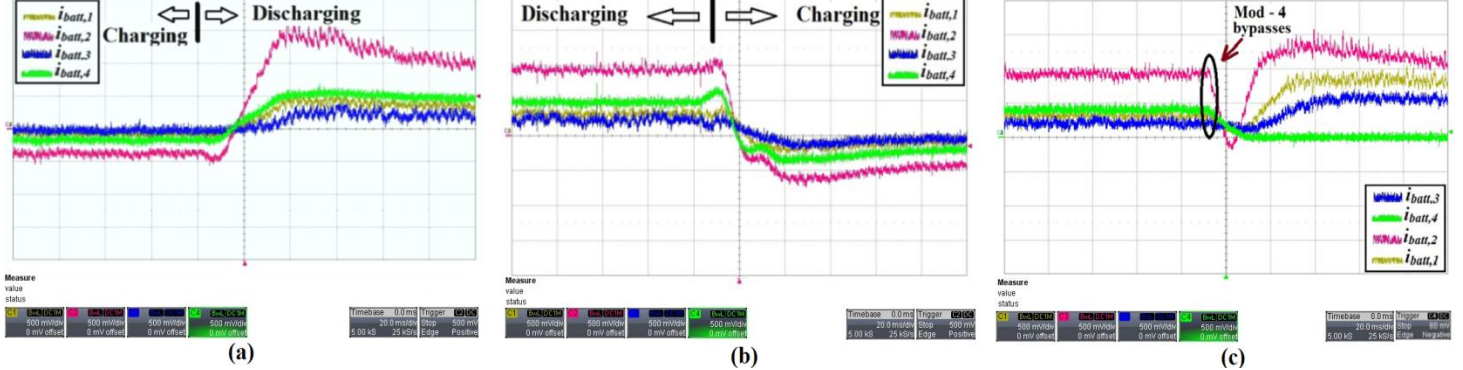

Fig 6 Experimental result of mode switching: a) charging to discharging, b) discharging to charging, c) module bypassing, scale time 20ms/div, module currents 5A/div
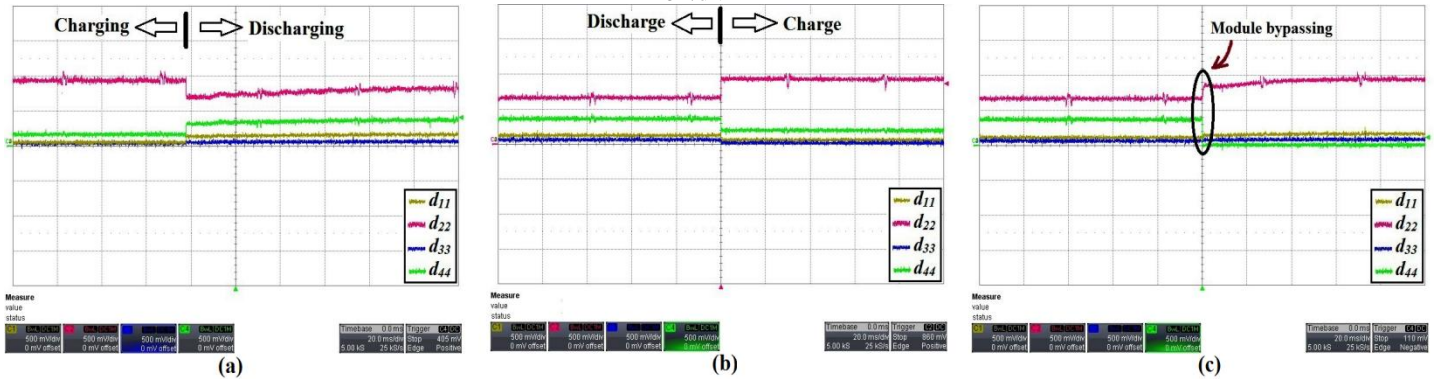

Fig. 7 Duty ratio distribution of T_1, T_{ii} a) charging to discharging, b) discharging to charging, c) module bypassing: Scale: duty ratio 0.5 /div, time 20ms/div

B. Distributed Power Sharing (Current Dynamics)

Mode – 1 zero to discharging mode: Fig 5b shows the experimental result for the distributed control scheme at the moment of connecting to the grid. It can be seen that the converter distinctly utilises the hybrid modules where the module currents are almost in 1:8 ratio. The module currents are dependent on the weighting factors. Table III shows the comparison of calculated and measured currents

Mode – 2 zero to charging mode (current dynamics): Fig 5c shows the experimental result when the converter switches to charging mode. The second module is charged at a significantly higher current than the remaining modules. Module currents are widely different (1:10 ratio exists between the highest and lowest module currents). The steady state values of module currents are presented in Table III.

Mode – 3 charging to discharging mode (current dynamics): Fig 6(a) shows the experimental result when the converter switches from charging mode to discharging mode. It is

important to note that the current sharing between the modules is different in charging and in discharging due to the differences in weighting functions between the two modes. The details are given in Table III.

Mode – 4 discharging to charging mode (current dynamics): Fig 6(b) shows the experimental result when the converter switches from discharging mode to charging mode. It is to be noted that the all the module currents in charging and discharging mode are different and the current sharing changes after switching from discharging to charging mode.

C. Module Bypassing (Current Dynamics)

Fig 6(c) shows the experimental result of module bypassing during discharging. In this experiment, module – 4 has been bypassed. The remaining modules clearly take a higher share of the currents to keep the power. A momentary drop in the currents occurs due to the sudden dip in V_{dc} but then recovers quickly. This shows the fault tolerance of the converter.

D. Duty ratio Distribution

The converter in Fig 1 operates in boost-buck fashion where the S_i, S_{ii} operates in PWM mode to form the module dc-link voltages and T_i, T_{ii} operates in PWM fashion to utilize the hybrid modules. Fig 7 shows how the duty ratios are used to change the power sharing during the transition of modes. Fig 7(a) shows the distribution of module duty ratio while switching from charging to discharging and Fig 7(b) shows the similar waveform while moving from discharging to charging mode. On the other hand, Fig 7(c) shows the module duty ratio distribution when module – 4 bypasses. It can be seen that the module duty ratios (d_{ii}) re-distributes among themselves to keep the overall duty ratio (d_{av}) constant all the time because the total dc-bus voltage (V_{dc}) is controlled to a desired value through a central voltage loop as shown in Fig 2.

E. Module voltage dynamics

Fig 8 shows the dynamics of module dc-link voltages ($V_{dc,i}$) at the start up. Note that all the voltages are equal in steady-state as expected from the design presented in section V after undergoing slightly different transient response.

Table III

COMPARISON OF CALCULATED AND EXPERIMENTAL MODULE CURRENTS

Cases	Initial SOC/OCV before changing a mode	Calculated current references	Measured steady-state module currents
Mode – 1	OCV_{O1} =11.21V OCV_{O2} =22.6V OCV_{O3} =8.08V OCV_{O4} =23.5V	$i_{batt,1}^* = 1.5A$ $i_{batt,2}^* = 11.5A$ $i_{batt,3}^* = 3A$ $i_{batt,4}^* = 3.9A$	$i_{batt,1} = 1.3A$ $i_{batt,2} = 10A$ $i_{batt,3} = 2.5A$ $i_{batt,4} = 3.5A$
Mode – 2	OCV_{O1} =12.8V OCV_{O2} =25.1V OCV_{O3} =7.4V OCV_{O4} =24.2V	$i_{batt,1}^* = - 0.6A$ $i_{batt,2}^* = - 6.1A$ $i_{batt,3}^* = - 0.48A$ $i_{batt,4}^* = - 2.0A$	$i_{batt,1} = - 0.5A$ $i_{batt,2} = - 5A$ $i_{batt,3} = - 0.55A$ $i_{batt,4} = - 1.8A$
Mode – 3	OCV_{O1} =13.27V OCV_{O2} =25.8V OCV_{O3} =7.66V OCV_{O4} =25.24V	$i_{batt,1}^* = 2.3A$ $i_{batt,2}^* = 9.5A$ $i_{batt,3}^* = 1A$ $i_{batt,4}^* = 3.2A$	$i_{batt,1} = 2.6A$ $i_{batt,2} = 9.6A$ $i_{batt,3} = 1.5A$ $i_{batt,4} = 3A$
Mode – 4	OCV_{O1} =12.33V OCV_{O2} =24.6V OCV_{O3} =7.55V OCV_{O4} =23.26V	$i_{batt,1}^* = - 0.9A$ $i_{batt,2}^* = - 4.8A$ $i_{batt,3}^* = - 0.5A$ $i_{batt,4}^* = - 2.1A$	$i_{batt,1} = - 0.7A$ $i_{batt,2} = - 4.8A$ $i_{batt,3} = - 0.4A$ $i_{batt,4} = - 1.9A$

F. Validation of overall control

Fig 9 shows the experimental results for grid side and dc-link side control system operation at a moment in time when the inverter is switched from the charging to discharging mode. It can be seen that the phase angle of the line side current changes with respect to the line voltage when the dc-link current (I_{dc}) moves from negative to positive. It is to be noted that the total DC-link voltage (V_{dc}) stays constant during the transition.

G. Converter Efficiency

The overall converter efficiency was measured in two steps: a) efficiency of the modular dc-dc converter consisting of four modules, b) efficiency of the overall grid-tie converter along with the inverter efficiency. The cascaded boost-multilevel buck converter from the experimental setup has a measured efficiency of around 96% at a 10 kHz switching frequency. The cascaded converter has a high efficiency because the LV Trench MOSFETs used in the H-Bridge module have a very low on-state resistance (R_{dson} = 8mΩ). The overall efficiency

of the converter was found to be around 92% when the inverter is included in the calculation, however there is scope to improve this using more efficient devices in the inverter.
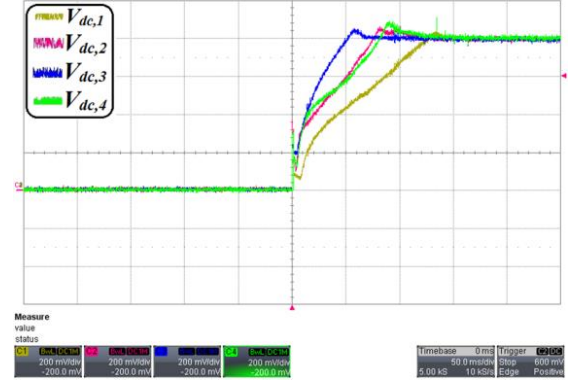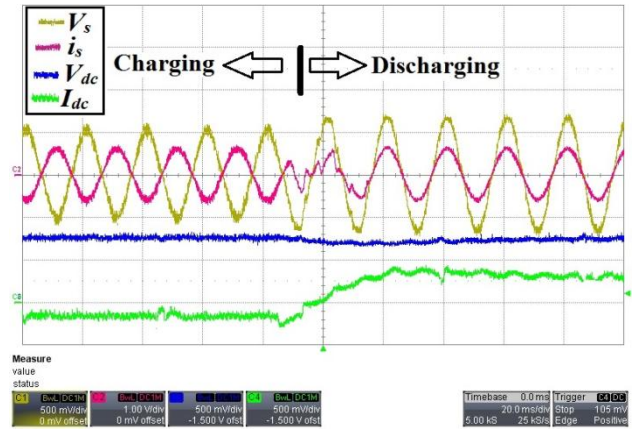

Fig 8 Capacitor voltage ($V_{dc,i}$) dynamics: time 50ms/div, voltage 20V/div

Fig. 9 Overall control dynamics: charging to discharging mode (time 20ms/div, grid voltage 100V/div, grid current 10A/div, DC-link voltage 100V/div, DC-link current 5A/div)

H. Validation of Charging/Discharging Trajectory

All the modules were started at different initial SOC and/or voltage levels. The converter was run for a long time using the distributed strategy. The state-of-charge (SOC) is plotted during discharging and charging in Fig 10 and Fig 11 respectively under normal conditions. A zero SOC corresponds to the minimum capacity condition and a unity SOC corresponds to the fully charged condition in this case. It can be seen that the module with a lower initial SOC has a larger slope compared to the module with a higher initial SOC during charging and vice-versa during discharging. All the module SOC's reach zero or unity at around the same time using the proposed weighting factor based strategy.

Capacity fade is an important practical phenomenon in second life application. In order to validate the proposed strategy under this condition, two identical batteries of the same voltage (12V) and capacity (10Ah) were put in parallel through a dc-breaker. Mid-way through the discharging experiment, one battery was disconnected through the breaker. As a result, the effective charge or capacity was halved while impedance was doubled, and this was picked up by the capacity estimator. The current sharing was affected due to this change because of the change in the weighting factors. This is shown Fig 12 where the current share taken by battery

– 1 is reduced while that taken by the remaining modules is increased and the discharging trajectory continues as expected. In this way, the proposed strategy remains valid.
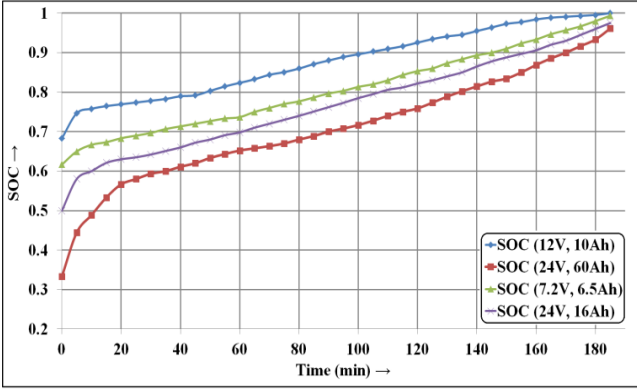

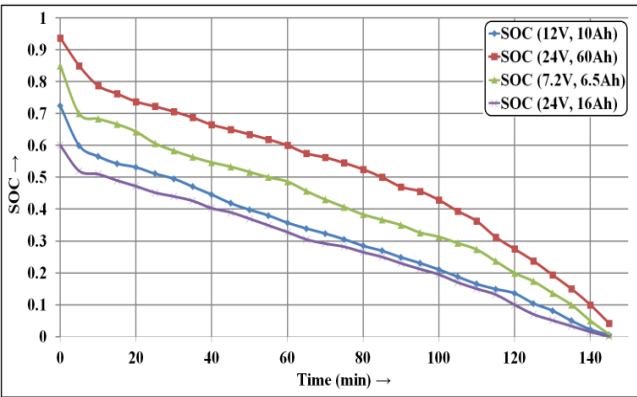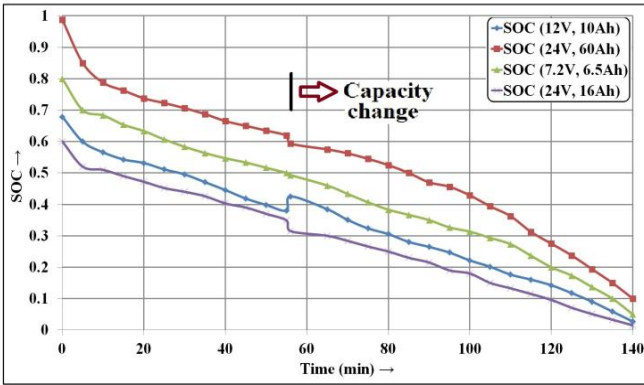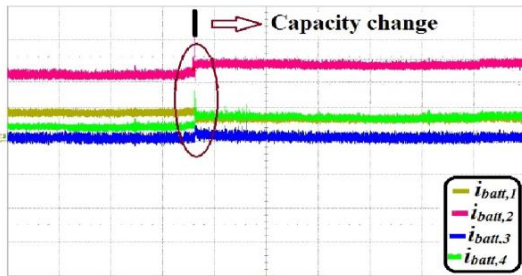Fig. 10 Experimental result of charging trajectory under normal condition

Fig. 11 Experimental resultsof discharging trajectory under normal condition

(a)

(b)

Fig 12 Experimental result of discharging trajectory under capacity fade: a) full discharging trajectory, b) current sharing (time 2s/div, current 5A/div)

VII. CONCLUSION AND FUTURE WORK

A modular boost- multilevel buck based converter topology and a module based distributed control architecture based on weighting function are proposed, analysed and experimentally validated to integrate any set of second life batteries to a grid-tie energy storage system and to optimally utilise them. The proposed converter is found to be efficient and is capable of utilising widely different battery modules characteristics using boost-buck control mode. The control structure is based on weighting factors which are dependent on module battery characteristics such as, initial SOC, voltage impedance and capacity in order to take account their different performances. The results show the suitability of the topology and control structure when widely different batteries are present. The application is focused on single-phase but the proposed converter structure and control architecture can be extended into three-phases and also other multi-modular energy systems.

APPENDIX – WEIGHTING FACTOR DERIVATION

The strategy adopted in this paper is to ensure that the charging/discharging trajectory of the hybrid battery modules during a charging or discharging cycle will all arrive at their maximum or minimum values at the same time. The following assumptions have been taken:

- A battery capacity has been taken as the maximum charge left (Q_{max} in C or Ah) that a battery can deliver to a load.
- A battery is modelled as an open circuit voltage (OCV) with series impedance (Z) → $V_{batt,i} = OCV_i \pm i_{batt,i} Z_i$.
- Each battery module have different initial SOC (or $OCV_{o,i}$) at start, different nominal voltages and also different capacity ($Q_{max,i}$).

A. Weighting Factor

The fundamental charge equation for a module is given by (A.1) where the Q_0 is the initial charged stored. Now assume, the module battery charge Q (t) is some function f (.) of its open-circuit voltage OCV (t):

$$Q\ (t) = Q_0 + \int_0^T i_{batt}\ dt = f(OCV(t)) \qquad (A.1)$$

Therefore,

$$f(OCV(t)) = f(OCV_o(t)) + \int_0^T i_{batt}\ dt \qquad (A.2)$$

Where, OCV_o is the measured module open-circuit voltage at time t=0 (V). This OCV_o indicates the initial SOC. For the charging/discharging strategy chosen at some time $T=T_{minmax}$ where the charging/discharging process must cease.

Therefore, $OCV\ (t)_{@T_{minmax}} = OCV_{minmax} \qquad (A.3)$

OCV_{minmax}: module maximum or minimum open-circuit voltage at time T_{minmax}. Under these conditions (A.2) becomes:

$$f(OCV_{minmax}) = f(OCV_o) + \int_0^{T_{minmax}} i_{batt}\ dt \qquad (A.4)$$

Re-arranging in terms of the module charging current gives:

$$\int_0^{T_{minmax}} i_{batt}\, dt = f(OCV_{minmax}) - f(OCV_o) \tag{A.5}$$

Equation (A.5) can be solved for an approximately constant charging/discharging current conditions as follows:

$$I_{batt} = \frac{f(OCV_{minmax}) - f(OCV_o)}{T_{minmax}} \tag{A.6}$$

Where I_{batt} is the signed magnitude of the constant charging/discharging current (A).

In equation (A.6), OCV_{minmax} should be known for a particular module based on pre-characterization and OCV_o can be measured taking the first sample instant of open circuit voltage (OCV) calculated from the battery model (= $V_{batt} \pm I_{batt} Z$) as a charge/discharge cycle begins.

However, in a typical grid support application, T_{minmax} will be unknown to the hybrid modules. To eliminate T_{minmax} from (A.6), the converter power balance equation can be used as shown below.

$$P = \sum_{k=1}^{n} V_{batt,k} I_{batt,k} \tag{A.7}$$

Where n is the number of active modules and each module k has a different voltage, $V_{batt,k}$ and current $I_{batt,k}$.

Now, substituting (A.6) into (A.7) for each module k, gives:

$$P = \sum_{k=1}^{n} V_{batt,k} \frac{f(OCV_{minmax,k}) - f(OCV_{o,k})}{T_{minmax}} \tag{A.8}$$

To find, say, $I_{batt,1}$ and eliminate T_{minmax} from (A.8) which is equal for all modules, substitute for T_{minmax} from (A.6):

$$P = \sum_{k=1}^{n} V_{batt,k} \frac{f(OCV_{minmax,k}) - f(OCV_{o,k})}{\left(\frac{f(OCV_{minmax,1}) - f(OCV_{o,1})}{I_{batt,1}}\right)} \tag{A.9}$$

Re-arranging (A.9) gives the desired module battery current:

$$I_{batt,1} = P\left(\frac{f(OCV_{minmax,1}) - f(OCV_{o,1})}{\sum_{k=1}^{n} V_{batt,k}(f(OCV_{minmax,k}) - f(OCV_{o,k}))}\right) \text{ or } \tag{A.10}$$

$$I_{batt,i} = P\left(\frac{f(OCV_{minmax,i}) - f(OCV_{o,i})}{\sum_{k=1}^{n} V_{batt,k}(f(OCV_{minmax,k}) - f(OCV_{o,k}))}\right) = P\omega_i \tag{A.11}$$

If a straight-line relationship is assumed between OCV (t) and Q (t) such as reported in [15], then $f(OCV)$ simplifies to:

$$OCV_k(t) = OCV_{min,k} + \frac{(OCV_{max,k} - OCV_{min,k})}{Q_{max,k}} Q_k(t) \tag{A.12}$$

Substituting, (A.12) in (A.11) gives the desired ω_i

$$\omega_i = \left(\frac{\left(\frac{OCV_{0,i} - OCV_{min,i}}{OCV_{max,i} - OCV_{min,i}}\right)Q_{max,i}}{\sum_{k=1}^{n} V_{batt,k}\left(\frac{OCV_{0,k} - OCV_{min,k}}{OCV_{max,k} - OCV_{min,k}}\right)Q_{max,k}}\right) discharge$$

$$\omega_i = \left(\frac{\left(\frac{OCV_{max,i} - OCV_{0,i}}{OCV_{max,i} - OCV_{min,i}}\right)Q_{max,i}}{\sum_{k=1}^{n} V_{batt,k}\left(\frac{OCV_{max,k} - OCV_{0,k}}{OCV_{max,k} - OCV_{min,k}}\right)Q_{max,k}}\right) charge \tag{A.13}$$

B. Parameter Estimation

The proposed sharing strategy requires two important parameters: a) initial OCV or SOC ($OCV_{0,i}$), b) capacity ($Q_{max,i}$). The $OCV_{0,i}$ in the weighting factor has to be updated at the end of a charging or discharging cycle. The battery capacity (or Q_{max}) has to be tracked during the operation because long term battery degradations will consequently affect this capacity. Apart from the capacity, the internal impedance (Z) is also prone to vary with the age and degradations. The variation of that acts as an indicative of power fade because the state-of-heath (SOH) of a battery is a combination of power fade and capacity fade as reported in [24] − [25]. Therefore, both the parameters are estimated during the converter operation to track the SOH online.

Impedance (Z) Estimation:
There are many methods to estimate the impedance of battery: a) a pulse based method [26] b) a ripple based online impedance method similar to [27] as described in Fig A.1, c) EIS based techniques [25]. The pulse power based method is straightforward but it requires the battery to be at rest for at least 2-5 minutes between the tests. This method has been used to find impedance of a battery as part of the pre-characterization tests prior to connecting a battery module to the system. However, it is difficult to provide a pulse current reference externally to the battery modules when the inverter connected energy storage system is providing the necessary grid support because the power command is decided by the inverter which is dependent on the grid side demand. EIS based methods are expensive and are suitable in off-line applications. On the other hand, the ripple based method described in Fig A.1 is valid when the power converter is running because it is based on the ripple part of the voltage and current to estimate the impedance under running conditions. The principle concept is to use the high frequency inductor ripple current of the associated dc-dc converter and corresponding high frequency ripple of the battery terminal voltage to calculate the internal impedance. Therefore, it is deemed more appropriate in this application because this ripple is always present during the converter operation. The switching frequency is in the order of multiples of kHz's, so it can be assumed that the *SOC/OCV* does not change significantly during such small switching interval. Two different equations can be written in each switching period: at t =0 and t = dT_s as shown below (where d represents the converter duty ratio and the $\pm$ refers to charging/discharging condition). The ripple part of the voltage and current are extracted through a low pass filter as shown in Fig A.2. The validation of the method is presented in Fig A.2 where an external impedance of 0.033Ω has been put in series with a 24V, 16Ah lead acid battery. It can be seen that the method is able to track the variation of impedance (both increase and decrease within 1 − 2%) and so can be used to track any power fade.

$$V_{batt_{max/min}} = OCV \pm i_{batt_{min/max}} Z \; at\; t = 0 \tag{A.14}$$

$$V_{batt_{min/max}} = OCV \pm i_{batt_{max/min}} Z \; at\; t = dT_s \tag{A.15}$$

$$Z = \left|\frac{(V_{batt\,max} - V_{batt\,min})}{(i_{batt\,max} - i_{batt\,min})}\right| = \frac{|(\Delta V_{batt})|}{|(\Delta i_{batt})|} \quad (A.16)$$
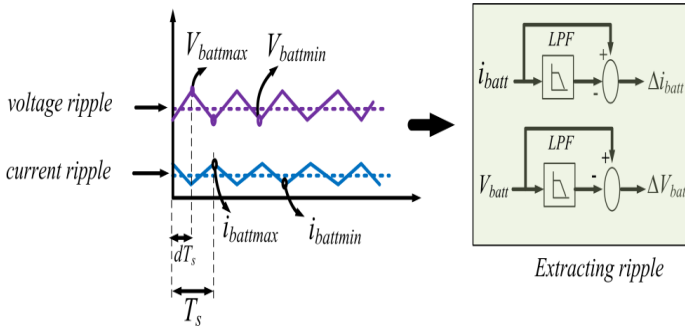

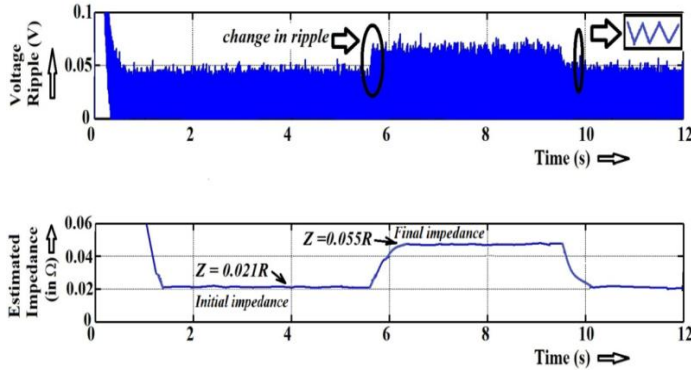Fig A.1 ripple based method to find impedance during converter operation

Fig A.2 Experimental observation of impedance estimation technique by putting an external resistance of 0.033Ω in series with a 24V battery

Capacity ($Q_{max,i}$) Estimation:

a) Step – 1: Obtain the impedance using the method described above.

b) Step – 2: Find the corresponding OCV using the battery model, i.e. $OCV = V_{batt} + i_{batt}Z$ (discharging) and $OCV = V_{batt} - i_{batt}Z$ (charging)

c) Step – 3: Determine the instantaneous SOC from a pre-characterized and pre-defined SOC-OCV look-up table or a derived function for each battery type

d) Step – 4: Once the SOC is determined from the OCV, the capacity of each module can be estimated using the following coulomb counting expression similar way as reported in [23]:

$$SOC\,(t) = SOC_0 - \frac{\int i_{batt}dt}{Q_{max}} \rightarrow Q_{max} = \frac{|\int i_{batt}dt|}{|SOC\,(t) - SOC_0|} \quad (A.17)$$

Moreover, the past researches show that the battery internal impedance (Z) is related to the battery capacity (Q_{max}) either through a linear relationship [24] or through a nonlinear relationship [28]. This means if one parameter changes there will be a subsequent change in the other. Therefore, both power and capacity fade are implicitly included in the formula. The combined SOH could be calculated directly using this method because both the quantities are estimated.

The proposed strategy is valid for various temperature because any variation of temperature causes the capacity Q_{max} and impedance (Z) to change because both are functions of temperature [28]. In this work, both are estimated through

online monitoring. For example, if the temperature of the modules were to reduce, then the impedance would increase and the capacity would reduce. This will result in a lower current share in the battery using the proposed strategy which would reduce the losses in the battery and help to cool the battery.

REFERENCES

[1] Vazquez, S.; Lukic, S.M.; Galvan, E.; Franquelo, L.G.; Carrasco, J.M., "Energy Storage Systems for Transport and Grid Applications," *Industrial Electronics, IEEE Transactions on* , vol.57, no.12, pp.3881,3895, Dec. 2010.

[2] Liaw, C.M.; Chiang, S. J., "Design and implementation of a single-phase three-wire transformerless battery energy storage system," *Industrial Electronics, IEEE Transactions on* , vol.41, no.5, pp.540,549, Oct 1994.

[3] Rahimi-Eichi, H.; Ojha, U.; Baronti, F.; Chow, M., "Battery Management System: An Overview of Its Application in the Smart Grid and Electric Vehicles," *Industrial Electronics Magazine, IEEE*, vol.7, no.2, pp.4,16, June 2013.

[4] Abusara, M.A.; Guerrero, J.M.; Sharkh, S.M., "Line-Interactive UPS for Microgrids," *Industrial Electronics, IEEE Transactions on*, vol.61, no.3, pp.1292,1300, March 2014.

[5] Lacey, G.; Putrus, G.; Salim, A., "The use of second life electric vehicle batteries for grid support," *EUROCON, Zagreb, 2013 IEEE* , vol., no., pp.1255,1261, 1-4 July 2013.

[6] Gladwin, D.T.; Gould, C.R.; Stone, D.A.; Foster, M.P., "Viability of "second-life" use of electric and hybrid electric vehicle battery packs," *Industrial Electronics Society, IECON 2013, Vienna, - 39th Annual Conference of the IEEE* , vol., no., pp.1922,1927, 10-13 Nov. 2013.

[7] Strickland, D.; Chittock, L.; Stone, D.A.; Foster, M.P.; Price, B., "Estimation of Transportation Battery Second Life for Use in Electricity Grid Systems," *Sustainable Energy, IEEE Transactions on* , vol.PP, no.99, pp.1,1.2014.

[8] Hui Li; Zhong Du; Kaiyu Wang; Tolbert, L.M.; Danwei Liu, "A Hybrid Energy System Using Cascaded H-bridge Converter," *Industry Applications Conference, 2006. 41st IAS Annual Meeting. Conference Record of the 2006 IEEE* , vol.1, no., pp.198,203, 8-12 Oct. 2006.

[9] Lu, X.; Sun, K.; Guerrero, J.M.; Vasquez, J.C.; Huang, L., "State-of-Charge Balance Using Adaptive Droop Control for Distributed Energy Storage Systems in DC Microgrid Applications," *Industrial Electronics, IEEE Transactions on* , vol.61, no.6, pp.2804,2815, June 2014.

[10] Poh Chiang Loh; Lei Zhang; Feng Gao, "Compact Integrated Energy Systems for Distributed Generation," *Industrial Electronics, IEEE Transactions on* , vol.60, no.4, pp.1492,1502, April 2013.

[11] Velasco de la Fuente, D.; Rodríguez, C.L.T.; Garcerá, G.; Figueres, E.; Gonzalez, R.O., "Photovoltaic Power System With Battery Backup With Grid-Connection and Islanded Operation Capabilities," *Industrial Electronics, IEEE Transactions on* , vol.60, no.4, pp.1571,1581, April 2013.

[12] Haihua Zhou; Bhattacharya, T.; Duong Tran; Siew, T.S.T.; Khambadkone, A.M. "Composite Energy Storage System Involving Battery and Ultracapacitor With Dynamic Energy Management in Microgrid Applications", *Power Electronics, IEEE Transactions on*, On page(s): 923 - 930 Volume: 26, Issue: 3, March 2011.

[13] Walker, G.R.; Sernia, P.C., "Cascaded DC-DC converter connection of photovoltaic modules," *Power Electronics, IEEE Transactions on*, vol.19, no.4, pp.1130, 1139, July 2004.

[14] Bratcu, A.I.; Munteanu, I.; Bacha, S.; Picault, D.; Raison, B., "Cascaded DC–DC Converter Photovoltaic Systems: Power Optimization Issues," *Industrial Electronics, IEEE Transactions on*, vol.58, no.2, pp.403,411, Feb. 2011.

[15] Kadri, R.; Gaubert, J-P; Champenois, G., "Nondissipative String Current Diverter for Solving the Cascaded DC–DC Converter Connection Problem in Photovoltaic Power Generation System," *Power Electronics, IEEE Transactions on* , vol.27, no.3, pp.1249,1258, March 2012.

[16] Montesinos-Miracle, D.; Massot-Campos, M.; Bergas-Jane, J.; Galceran-Arellano, S.; Rufer, A., "Design and Control of a Modular Multilevel DC/DC Converter for Regenerative Applications," *Power Electronics, IEEE Transactions on* , vol.28, no.8, pp.3970,3979, Aug. 2013.

[17] Uno, M.; Tanaka, K., "Single-Switch Multioutput Charger Using Voltage Multiplier for Series-Connected Lithium-Ion

Battery/Supercapacitor Equalization," *Industrial Electronics, IEEE Transactions on* , vol.60, no.8, pp.3227,3239, Aug. 2013.

[18] Hong-sun Park; Chong-Eun Kim; Chol-Ho Kim; Gun-Woo Moon; Joong-Hui Lee, "A Modularized Charge Equalizer for an HEV Lithium-Ion Battery String," *Industrial Electronics, IEEE Transactions on* , vol.56, no.5, pp.1464,1476, May 2009.

[19] Chung-Ming Young; Neng-Yi Chu; Liang-Rui Chen; Yu-Chih Hsiao; Chia-Zer Li, "A Single-Phase Multilevel Inverter With Battery Balancing," *Industrial Electronics, IEEE Transactions on* , vol.60, no.5, pp.1972,1978, May 2013.

[20] Maharjan, L.; Inoue, S.; Akagi, H.; Asakura, J., "State-of-Charge (SOC)-Balancing Control of a Battery Energy Storage System Based on a Cascade PWM Converter," *Power Electronics, IEEE Transactions on* , vol.24, no.6, pp.1628,1636, June 2009.

[21] Femia, N.; Lisi, G.; Petrone, G.; Spagnuolo, G.; Vitelli, M., "Distributed Maximum Power Point Tracking of Photovoltaic Arrays: Novel Approach and System Analysis," *Industrial Electronics, IEEE Transactions on* , vol.55, no.7, pp.2610,2621, July 2008.

[22] Alajmi, B.N.; Ahmed, K.H.; Finney, S.J.; Williams, B.W., "A Maximum Power Point Tracking Technique for Partially Shaded Photovoltaic Systems in Microgrids," *Industrial Electronics, IEEE Transactions on* , vol.60, no.4, pp.1596,1606, April 2013.

[23] Einhorn, M.; Conte, F.V.; Kral, C.; Fleig, J., "A Method for Online Capacity Estimation of Lithium Ion Battery Cells Using the State of Charge and the Transferred Charge," *Industry Applications, IEEE Transactions on* , vol.48, no.2, pp.736,741, March-April 2012.

[24] Pattipati, B.; Sankavaram, C.; Pattipati, K.R., "System Identification and Estimation Framework for Pivotal Automotive Battery Management System Characteristics," *Systems, Man, and Cybernetics, Part C: Applications and Reviews, IEEE Transactions on* , vol.41, no.6, pp.869,884, Nov. 2011.

[25] Pattipati, B.; Pattipati, K.; Christopherson, J.P.; Namburu, S.M.; Prokhorov, D.V.; Liu Qiao, "Automotive battery management systems," *AUTOTESTCON, 2008 IEEE* , vol., no., pp.581,586, 8-11 Sept. 2008.

[26] Coleman, M.; Lee, C.K.; Hurley, W.G., "State of Health Determination: Two Pulse Load Test for a VRLA Battery," *Power Electronics Specialists Conference, 2006. PESC '06, Jeju,. 37th IEEE* , vol., no., pp.1,6, 18-22 June 2006.

[27] Huang, W.; Abu Qahouq, J., "An Online Battery Impedance Measurement Method Using DC-DC Power Converter Control," *Industrial Electronics, IEEE Transactions on* , vol.PP, no.99, pp.1,1.

[28] Tsujikawa, T.; Yabuta, K.; Matsushita, T., "Development of VRLA battery capacity estimation system," *Telecommunications Energy Conference, 2007. INTELEC 2007. Rome, 29th International* , vol., no., pp.788,793, Sept. 30 2007-Oct. 4 2007.